

2011

Microspike Based Chemical/Electric Thruster Concept for Versatile Nanosat Propulsion

Anthony Cofer
Purdue University

A Venkatraman
Purdue University

Alina A. Alexeenko
Purdue University - Main Campus, alexeenk@purdue.edu

Follow this and additional works at: <http://docs.lib.purdue.edu/aaepubs>



Part of the [Engineering Commons](#)

Recommended Citation

Cofer, Anthony; Venkatraman, A; and Alexeenko, Alina A., "Microspike Based Chemical/Electric Thruster Concept for Versatile Nanosat Propulsion" (2011). *School of Aeronautics and Astronautics Faculty Publications*. Paper 23.
<http://dx.doi.org/10.2514/6.2011-5921>

This document has been made available through Purdue e-Pubs, a service of the Purdue University Libraries. Please contact epubs@purdue.edu for additional information.

Microspike Based Chemical/Electric Thruster Concept for Versatile Nanosat Propulsion

Anthony Cofer[†], A. Venkatraman[†] and Alina Alexeenko^{*}

School of Aeronautics & Astronautics, Purdue University, West Lafayette, IN 47907

Small spacecraft that can be categorized as microsats, nanosats, and picosats has a strong potential for wide applications in communication, scientific experiments, and space exploration. In order to combine the advantages of both electric and chemical propulsion thrusters, a dual-mode microspike based thruster concept is proposed. For a fixed input power, it can operate in either a high-Isp mode or a high-thrust mode depending on the propulsive maneuver requirements. The hybrid thruster consists of a plug-annular cold or heated gas thruster in the chemical mode and a field emission thruster housed within the plug operating in the electric mode using a metallic propellant. The direct simulation Monte Carlo (DSMC) technique and the particle-in-cell technique are used to model the two different modes to estimate performance parameters of the thruster. The DSMC simulations show that the microspike nozzle can provide an improved specific impulse (Isp) at low Reynolds numbers when compared to a straight orifice or converging-diverging nozzle. The PIC simulations for the field emission thruster are shown to compute the current density, ion beam density, ion beam velocities and, hence, specific impulse and thrust accurately for conditions corresponding to earlier published experiments.

Nomenclature

C_{div}	=	correction factor
dA	=	increment of area
F	=	force or thrust
g	=	standard gravity
I	=	current
I_{sp}	=	specific impulse
m	=	mass
p	=	pressure
q	=	charge
R	=	specific gas constant
R_x	=	reaction force
T_0	=	stagnation temperature
T_x	=	x-component of temperature
u	=	axial velocity
v_e	=	effective velocity
γ	=	ratio of specific heats
ΔV	=	electrostatic potential
ρ	=	density

I. Introduction

The utility of nano and picosatellites is currently greatly restricted by limitations in their ability to maneuver and reorient themselves^[1]. Mass and volume constraints make miniaturization of conventional propulsion systems impractical for small spacecraft as performance degrades at reduced scales.

[†]Graduate Student, Student Member

^{*}Assistant Professor, Senior AIAA Member

Chemical propulsion systems for small spacecraft suffer from viscous losses inherent in low Reynolds number flows. Electric propulsion is an alternative as I_{sp} 's in 1,000s of seconds are common for many configurations but so far are restricted to thrust levels in the micro-Newton range due to high power consumption. However, having separate electric and chemical microthrusters to gain high I_{sp} and high thrust at low power would increase mass, size, and complexity of the vehicle negating any gain in performance. These considerations make dual-mode microthrusters especially attractive.

One application of such electric/chemical microthruster could be for active removal of large-mass space debris visualized in Fig. 1. The nanosatellite uses a dual-mode microthruster to reduce orbit lifetime of space junk by the reactive force generated by solar ablation.^[2] Preliminary studies^[3] using the direct simulation Monte Carlo method have shown that plug-annular chemical (PAC) micronozzle offers higher thrust than conventional designs due to a better utilization of pressure thrust. I_{sp} has been increased by more than 100% over converging-diverging nozzles at low Reynolds numbers.

In Fig. 2 the inert plug is replaced with an active field effect electric propulsive device (FEEP)^[4,5] such that a dual mode microthruster is obtained possessing the desired qualities of high I_{sp} coupled with high thrust. A microthruster of this type would be ideally suited for attitude control applications on spacecraft massing tens of kilograms. Minuscule adjustments could be made using the high resolution FEEP mode as well as high total impulse maneuvers if a longer duration is acceptable.

The dual-mode microthruster combines a field-emission electric propulsion (FEEP)^[4,5] mode with an $I_{sp} > 1000$ s for input powers < 10 W along with a chemical thruster based on a plug-annular micronozzle (PAM).^[6] Other electric propulsion options such as the MEMS-based electrospray thruster arrays^[7] can also be implemented in conjunction with the chemical microspike thruster.

The dual-mode microthruster concept is well suited for a number of applications including missions with very limited power budgets such as to the outer planets where large amounts of solar power are unavailable.

The FEEP mode has the ability to provide impulse resolutions of $0.01 \mu\text{N}\cdot\text{s}$ to maintain attitude control en route and the cold gas mode would provide the higher skew rates required for planetary fly-by. Another application could be in extraterrestrial mapping allowing orientation of a spacecraft to be changed without reaction wheels that have to be periodically de-saturated. The force is applied at the same points reducing the complexity and mass of having separate low and high power thrusters. The main goal of this paper is to develop a computational framework of tools that will help to formulate a performance model to optimize and design the dual-mode thruster by using the particle-in-cell (PIC) method for the FEEP mode and the direct simulation Monte Carlo (DSMC) method for the cold gas PAM mode.

The cold/warm gas chemical mode would be available when high slew rates are needed for a fast alignment such as the initial orbit insertion or a planetary flyby. This device could also be used as a main drive for nanospace-craft of

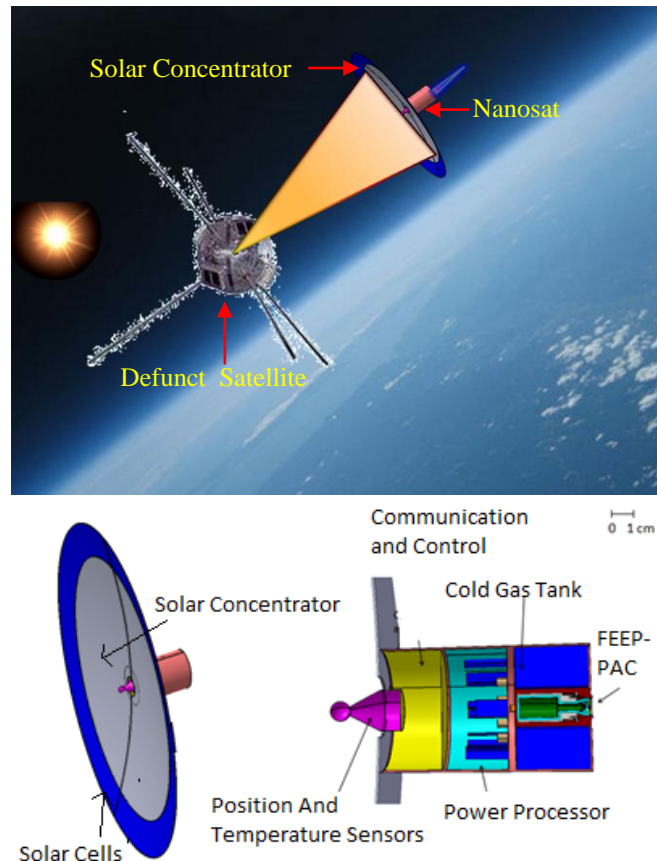


Figure 1. Nanosat based removal of space debris using focused solar ablation^[2]. The proposed electric/chemical micropropulsion system is enabling nanosat maneuvering and precise station keeping.

up to several kilograms mass as it combines high delta V from the FEEP with substantial short term acceleration. A comparison of such a device with current micropropulsion options is given in Table 1.^[8]

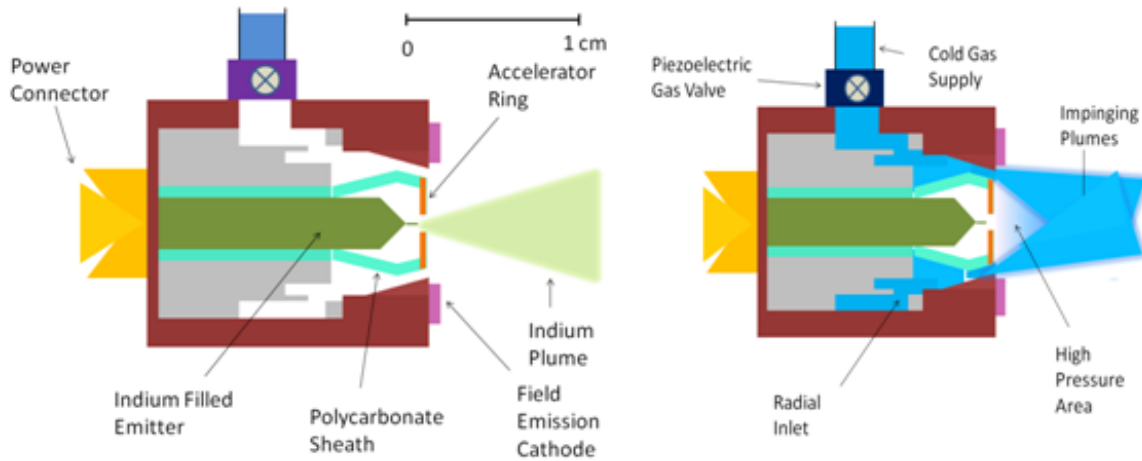


Figure 2. Propellant flow for microthruster in FEEP mode (left) and chemical mode (right)

Table 1. Micropropulsion Options

	Thrust	Isp	Power	Voltage	Size	Mass
Hall/Ion	1-20 mN	1000-3700s	50-300 W	100-1000 V	$\leq 5 \text{ cm}^3$	$\leq 1 \text{ kg}$
FEEP/Colloid	$1\mu\text{-}1.5\text{mN}$	450-9000s	1-100 W	1-10 kV	$\leq 800 \text{ cm}^3$	0.1-1 kg
Electromagnetic	0.03-2mN	200-3000s	$\leq 10 \text{ W}$	kV	--	0.06-0.5 kg
Electrothermal	$\leq 5 \text{ mN}$	50-250s	5-300 W	1-10 V	$1\text{-}25 \text{ cm}^3$	0.1-1kg
Cold Gas	0.5-50mN	40-80s	$< 1 \text{ W}$	$< 20 \text{ V}$	$0.1\text{-}10\text{cm}^3$	0.01-0.5kg
Liquid	$1\mu\text{-}200\text{mN}$	100-315s	--	--	$0.1\text{-}10\text{cm}^3$	0.01-0.5kg
Dual-Mode	$0.01\mu\text{-}1\text{mN}$	50-6000s	$< 10 \text{ W}$	4.5-10 kV	$0.1\text{-}10\text{cm}^3$	0.01-0.5kg

None of the other systems represented possess all three attributes of low power, high resolution, and the thrust range promised by the dual mode design. Absence of highly stressed components and simplicity of operation promises fewer failure modes than with more complex configurations.

Another benefit to this dual-mode type thruster is the redundancy option. The cold gas system could provide impulses of $0.1 \mu\text{N}\cdot\text{s}$ by virtue of a precision piezoelectric valve. This would mean loss of the high Isp provided by the FEEP but could be used if the high voltage supply fails or propellant is exhausted. Also, if power is diverted from other systems, the FEEP's thrust could be increased well into the $100 \mu\text{N}$ range. Once again this would lower Isp but this overlap of operating ranges means that the lifetime of a mission could be extended until all propellant is consumed.

II. Microspike Concept

A. Background and Theory

Plug-annular micronozzles or microspikes is a novel concept for increasing the specific impulse of cold gas and chemical microthruster^[6]. Conventional macroscale bipropellant chemical or cold-gas propulsion systems commonly use gas expansion through converging-diverging de Laval nozzles. Such nozzles are employed to achieve supersonic flow velocities thereby converting a larger amount of gas internal energy into the kinetic energy and thrust. Traditional space propulsion systems operate with high stagnation pressures and sufficiently large length scales resulting in very high Reynolds numbers and thin boundary layers. Micronozzles for cold gas and chemical microthrusters have much smaller length scales and, thus, operate at low Reynolds numbers, typically $Re < 500$. At these low Reynolds numbers, viscous losses in the wall boundary layer result in a large subsonic portion of the flow and a decreased thrust efficiency. With the microspike arrangement throat area and expansion ratio can be conserved with less wall surface area.

The total thrust of chemical propulsion systems operating in low-Reynolds number conditions is comprised of the three terms as follows:

$$F = \left\{ \int_A \left(\rho \bar{u}^2 + P \frac{T_x}{T} \right) dA \right\}_{jet} + \left\{ \int_A R_x dA \right\}_{ext} \quad (1)$$

Jet Thrust Pressure Thrust Reaction on Ext Surfaces

where A is the nozzle exit control area, ρ is density, u is axial velocity, T_x is the temperature component in x -direction which can be different from the total temperature T due to rarefied flow at low-Reynolds number conditions, R_x is the reaction force on any walls at the thruster exit cross-section, p is the thermodynamic pressure. For high Reynolds number operation the first term is dominating the thrust, however, at low Reynolds numbers the pressure and reaction force contributions are considerable because flow velocity is decreased due to viscous losses.

The purpose of the plug-annular micronozzle is to utilize a configuration containing a centerline body to enhance thrust performance at low Reynolds numbers. The use of center-body in a nozzle is akin to aerospike nozzles with their pressure-compensating ability. However, utilizing a center-body for microthrusters allows for better exploitation of the pressure and reaction forces. In particular, creating an annular jet expanding toward its center and thus creating a higher pressure at the outer surface of the centerbody, as seen in Fig. 3, allows enhancement of thruster performance.

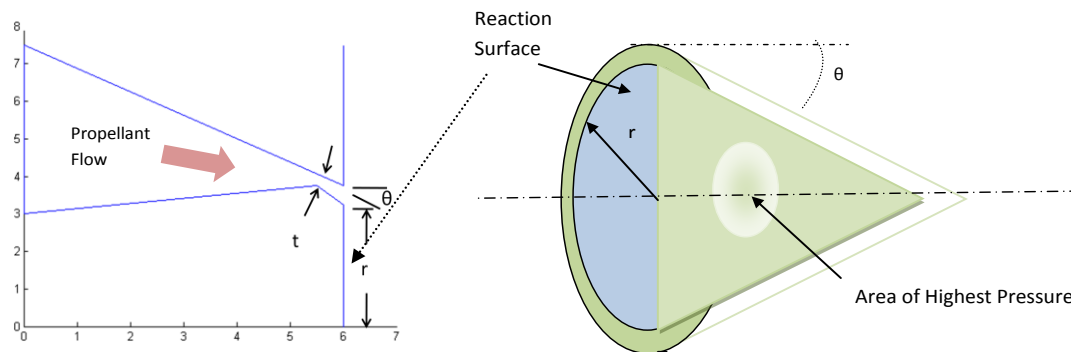


Figure 3. Axi-symmetric plug annular nozzle - bisected profile (left) conical impinging jet profile (right)

B. Propellant Selection

Table 2 lists the physical properties of various cold gas thruster propellants that were considered in this study and also the ideal Isp with the included center body effect for low Reynolds number flows based on numerical results with monatomic gases. The specific impulses for diatomic gases are estimated to be within 10% of monatomic values. Low molecular weight gases such as hydrogen and helium have high theoretical specific impulses that can exceed those of monopropellants but their extremely low densities result in prohibitively large and massive storage tanks. Higher molecular weight gases such as methane and nitrogen are more compact to store but also achieve significantly lower specific impulses. Ammonia (NH_3) which can be stored as a liquid at relatively low pressures, is an ideal candidate for the cold gas PAM mode propellant with an Isp comparable to methane but over three times its liquid density. Therefore, NH_3 is chosen as the propellant for the cold gas PAM mode.

Table 2. Comparison of properties of various propellants considered for the PAM mode.

Propellant	Density kg/m ³ (g/mol) @293 K 5000 psi	Ratio of Specific Heats	Molecular Weight g/mol	Molecular Hard Shell Diameter ^[9] $\times 10^{10}$ m
Hydrogen	28.4	1.40	2	2.88
Helium	56.7	1.67	4	2.13
Methane	(l) 226	1.30	16	2.28
Argon	565.3	1.67	40	4.11
Nitrogen	396	1.40	28	4.11
Ammonia	(l) 682	1.30	17	5.96

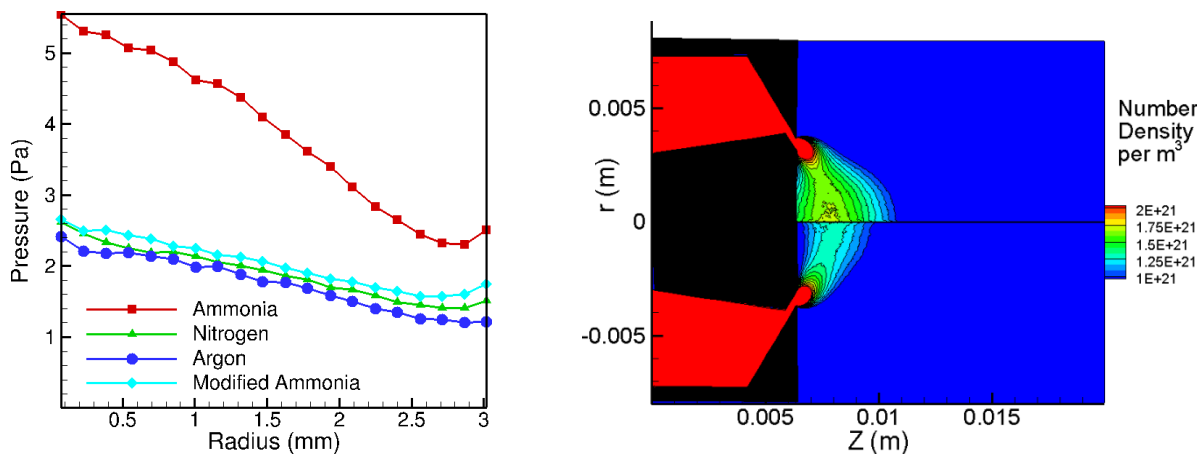


Figure 4. Pressure profile of gases across PAM reaction surface (left) and number density of ammonia (top right) vs modified ammonia (bottom right). Plug-Annular Nozzle 3.1 mm radius; 60 deg. Jet; Ammonia- top (both sides) modified Ammonia bottom (both sides); 1 mg/s flow rate; 8.66 mm² total throat area; 294K inlet temperature

Pressure profiles across the reaction surface of a microspike nozzle were generated with data from DSMC simulations using various gases with consistent mass flow and geometry. A hypothetical propellant was created as well which had all the properties of ammonia except diameter which was that of nitrogen in order to examine the effect of cross section change. Surface pressure profiles, where radius is defined in Fig 2, for these gases have been plotted in Fig 4, which includes a number density contour plot showing the population discrepancy between ammonia and its imaginary cousin.


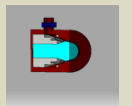
Pressure developed across the reaction surface is thus dependent primarily upon molecular diameter and is nearly independent of molecular weight which is the paramount parameter for momentum thrust.

C. Thrust Performance Comparison of PAC with State-of-the-art Cold/Heated Gas Thrusters

A comparison with three commercial microthrusters is found in Table 3. Some have thrust resolutions of several milliNewtons limiting their usefulness in ultra small spacecraft which may require microNewton-second impulses.

The PMT design allows thrusts in the microNewton range but uses a solenoid activated proportional valve which increases mass. The results shown for the microspike nozzle are from preliminary DSMC simulations without any optimization for chamber pressure, area ratio, or temperature enhancement.

Table 3. Comparison of commercial microthrusters

Model	Isp (s)	Mass (g)	Thrust Range (μN)	Power Consumption (W)	Propellant	
Bradford Engineering PMT ^[11]	>60	<175	1-2000	<4.5	N ₂	
Moog 58X125a ^[12]	65	9	4400	10	N ₂	
Marotta Cold Gas ^[13]	65	<70	50,000 - 2,360,000	10	N ₂	
PAC	80-93	<10	200-9,000	<0.1	NH ₃	

D. Preliminary Modeling Results

Three types of microthruster nozzles were compared: sonic orifice, converging-diverging, and the microspike. Nozzle profiles and general flow schematic of these can be seen in Fig 5. Figures 6 and 7 show contours of pressure and z-velocity respectively. They were obtained using the SMILE^[10] DSMC software system with a 0.8 by 2.0 cm

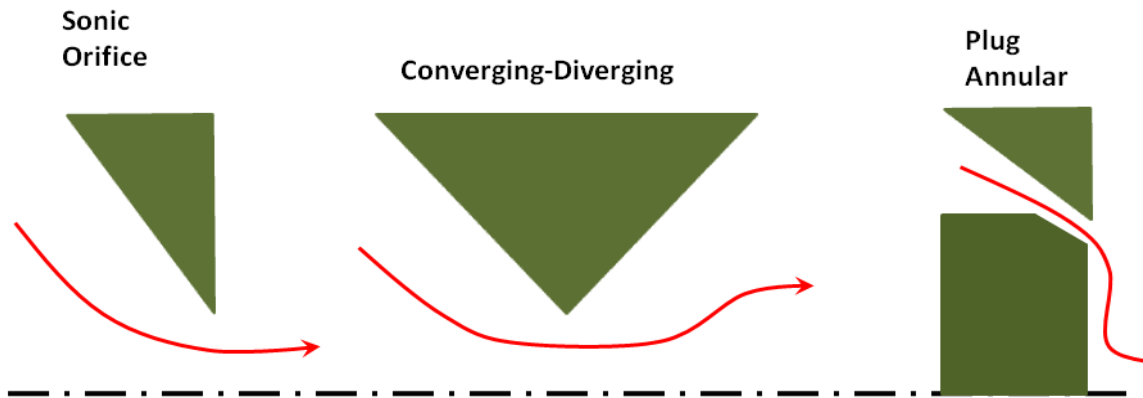


Figure 5. Schematic showing the various nozzle configurations considered in this work.

axi-symmetric domain incorporating 160 by 400 cells. Time steps were 15 ns with a total of 300,000 to 1,200,000 steps used for sampling of macroscopic parameters such as density, velocity, pressure and temperature components. Ammonia propellant was simulated using a variable hard sphere model including vibrational temperatures and rotational and vibrational relaxation factors. The computations show the extra thrust gained from the high-pressure area acting on the plug face in addition to the momentum thrust from the jet.

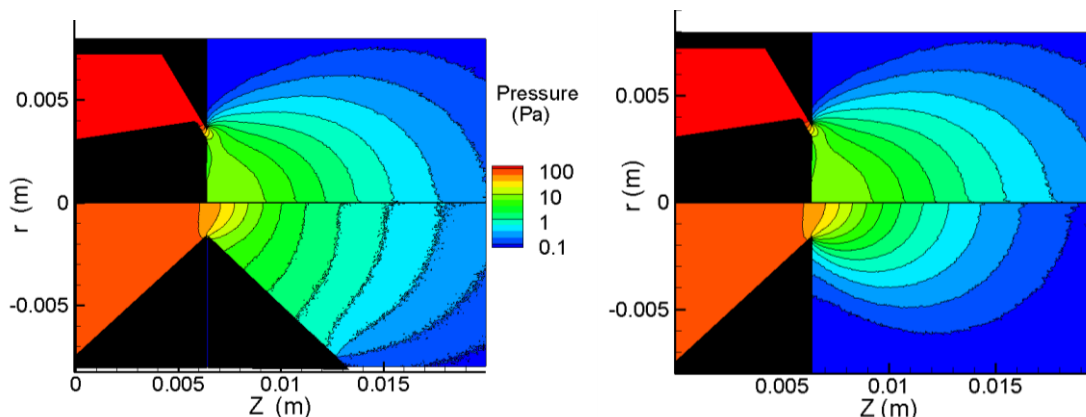


Figure 6. Pressure distribution for plug annular nozzle top (both sides) vs converging-diverging nozzle (bottom-left); sonic orifice (bottom right) 1 mg/s flow rate; 8.66 mm² total throat area; ammonia@294k

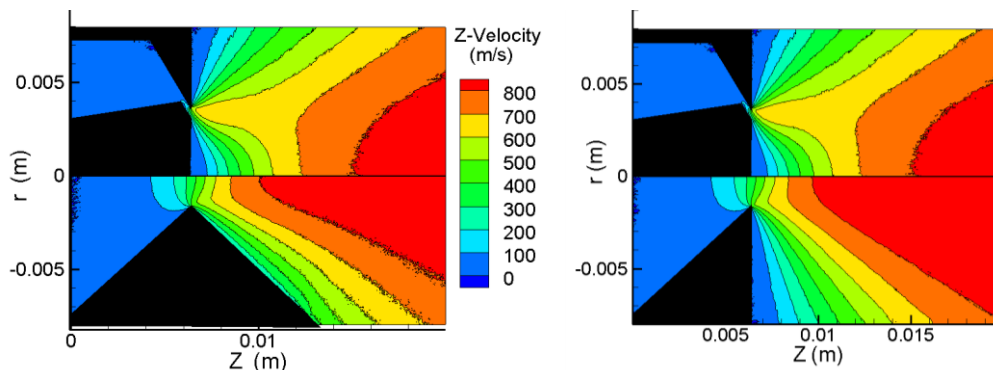


Figure 7. X-velocity distribution for plug annular nozzle top (both sides) vs converging-diverging nozzle (bottom-left); sonic orifice (bottom right) 1 mg/s flow rate; 8.66 mm² total throat area; ammonia@294k

The increase in I_{sp} due to pressure thrust can be seen in Fig. 8. At mass flow rates of 0.1 to 10 mg/s of ammonia at 294 K and the geometries seen in Figures 2 and 3, the microspike has the advantage over conventional designs. At higher flow rates performance is still comparable to the converging-diverging nozzle. At mass flow rates less than 0.05 mg/s all nozzles behaved similarly such that the simpler sonic orifice would be the nozzle of choice. Between 0.1 and 1 mg/s the converging diverging nozzle was slightly more efficient due to a T_x/T ratio exceeding unity at the nozzle exit in conjunction with significant exit pressure. The I_{sp} of the plug-annular nozzle was the highest over 1 mg/s flow rate; up to an 8 s increase over the converging-diverging design by increased pressure thrust on the reaction surface of the PAC with reduced T_x/T ratio at the C-D nozzle exit as seen in Figure 9. If mass flow were to be increased the I_{sp} 's of both designs would converge on the isentropic limit allowed by their respective expansion ratios, not exceeding 112.4 s from the jet at 294K found by^[3]

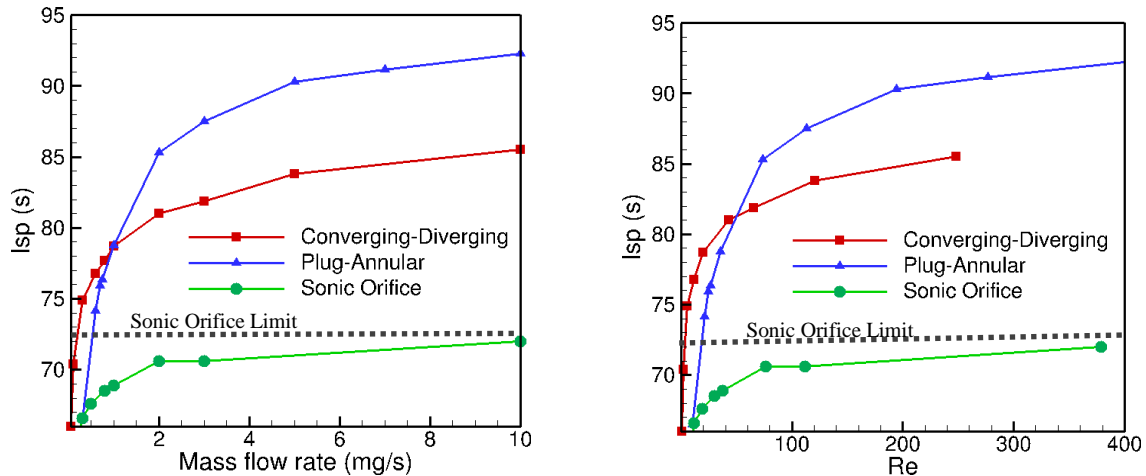


Figure 8. Isp vs mass flow rate (left) and Reynolds number (right) for three nozzle designs

$$Isp = \frac{\sqrt{\frac{2RT_0\gamma}{\gamma-1}}}{g} \quad (2)$$

the limit of a perfectly expanded nozzle, and on jet angle for the PAM. At mass flow rates greater than 2 mg/s the Isp of the sonic orifice approached its ideal value of 72.6 seconds at this temperature found by^[3]

$$Isp = \frac{\sqrt{\frac{2RT_0(\gamma+1)}{\gamma}}}{g} \quad (3)$$

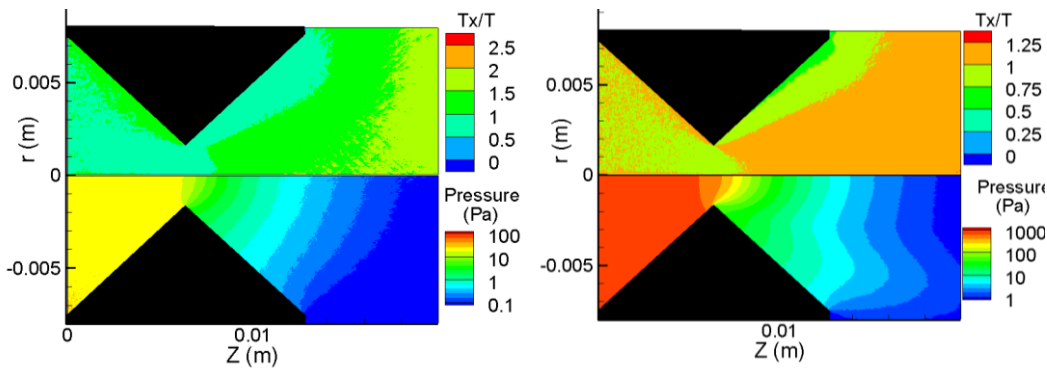


Figure 9. Tx/T ratio (top) and pressure (bottom) distributions for converging-diverging nozzle at 0.3 mgs (left) and 10 mgs (right) flow rates of ammonia@294K

Previous simulations with microspike nozzles using Argon propellant have produced Isp's of over 100 seconds over twice that obtained with a sonic orifice^[8]. Properly optimized ammonia propellant should provide Isp's in the range of 150 seconds due to lower molecular weight and larger diameter.

The use of ammonia propellant provides the benefit of not only lower molecular weight, increasing jet thrust, but has a liquid density of 0.6 g/cm³ at 10 bar at room temperature which is higher than methane (0.4 g/cm³) in its liquid state and eliminates the necessity for cryogenic storage measures used with noble gases or nitrogen. The mass for microspike is calculated assuming a 2 cm length by 2 cm diameter thruster assembly size. The thrust levels correspond to the values of Isp vs mass flow from figure 4. Piezoelectric valve is based on model LFPA8000120H from The LEE Company.

III. Integrated FEEP

The FEEP mode accelerates ions extracted from the surface of a liquid metal while the PAM mode expands the cold gas to provide the thrust. The thrust in the FEEP mode is given by

$$F = C_{div} I \sqrt{2m\Delta V/q} \quad (4)$$

where I is the current in amperes, V is the potential difference through which the ions are accelerated, q is the charge on the ion and m is the mass of the ion. Here, C_{div} is a correction factor that accounts for the divergence of the ion beam.

As with any thruster, the propellant selection is a critical step for the FEEP/PAM dual-mode thruster as well and the choice of propellants for both modes has to be made. For the FEEP mode, various liquid metals including those which were considered in the past for pure FEEP thrusters were considered. Properties of liquid metals that can be used as possible FEEP propellants are listed in Table 4. Indium is a good candidate FEEP propellant mainly because of its superiority with respect to contamination when compared to other metals such as Rubidium and Cesium. Bismuth was not considered because of its higher melting temperature and significantly higher molecular weight and hence lower Isp . The ideal Isp for the FEEP mode without accounting for the beam divergence effects is given by

$$Isp = \frac{v_e}{g} = \sqrt{\frac{2q\Delta V}{mg^2}} \quad (5)$$

Unlike other metallic propellants, Indium does not require complex isolation procedures as well as sealed environments which would make it particularly difficult to combine these with the cold-gas mode. The proposed use of Indium as FEEP propellant makes it possible to combine the FEEP thruster directly with the chemical thruster while eliminating propellant isolation requirements. This could lead to a potential decrease in the cost of development and fabrication of such a thruster. Also, Indium is commonly used in commercial electronics and is not a prohibitively expensive propellant on the scales required for a microthruster.

Table 4. Comparison of properties of various propellants considered for the FEEP mode.

	Atomic Number	Molecular Mass (g/mol)	Work Function (eV)	Melting Point (K)	Reactivity with oxygen
Cesium	55	133	2.14	302	High
Rubidium	37	85.5	2.26	312	High
Bismuth	83	209	4.34	545	Low
Indium	49	114	4.09	430	Low

As part of the computational framework that can model the dual-mode chemical/electric thruster, we present results obtained using numerical simulations for the FEEP component. The simulations are performed using the particle-in-cell/Monte Carlo collisions (PIC/MCC) method[14] which is a method used widely for the simulation of plasma, ion and electron beams in various applications. The results presented here do not consider the neutral vapor flow of Indium which is high particularly for the higher currents and hence higher thrust values. The absence of neutrals in the simulations imply that the ion-neutral interactions including charge exchange collisions which are likely to play a major role in determining the beam divergence are not considered. The effects of Coulomb collisions are also not included.

The simulation set-up considered is very similar to that in the experimental work by Tajmar et.al[4] and it consists of a plume shield apart from the emitter and accelerator configuration. The accelerator is always biased at 0 V whereas a positive potential is applied to the emitter. Figure 11 shows a schematic of the set-up used in numerical simulations including the boundary conditions. The accelerator plane is at a distance of 0.2 mm from the emitter tip. The PIC simulations were performed using the 2D/axi-symmetric code XOOPIC[15] developed at the University of Berkeley. The emitter was taken to be a cylinder of length 0.6 mm and radius 80 μm which is a reasonable assumption. A beam source was used to introduce ions of mass 1.9093E-25 kg corresponding to that Indium into the computational domain at every timestep.

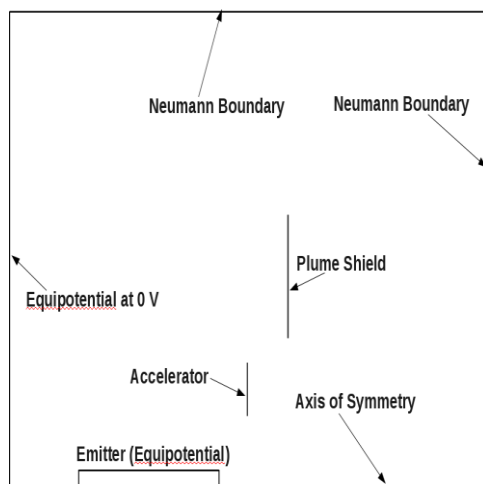


Figure 11. Schematic of the computational domain used for the PIC simulations along with the boundary conditions used.

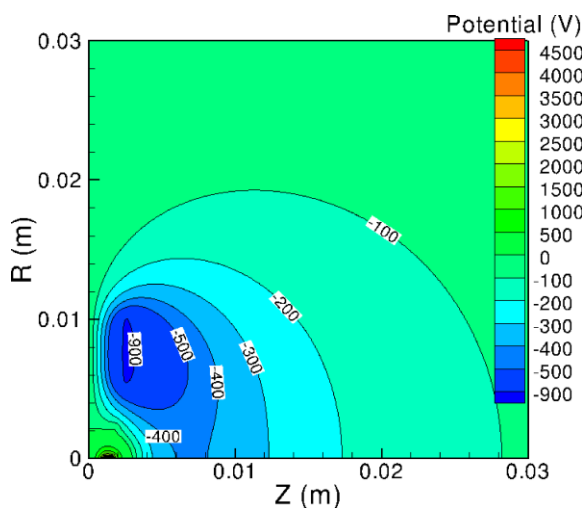


Figure 10. Contours of potential for the thruster operating in FEEP mode

The open boundaries were set as Neumann boundaries given by $\partial\phi/\partial n=0$ where n is r or z depending on whether the top or right boundary is considered. The domain size was fixed as $0.06\text{ m} \times 0.06\text{ m}$. The ratio of real to simulated number of particles is chosen as 1×10^3 . In reality, the emitter current is completely determined by the applied emitter voltage but at the present stage, the ion production process is not modeled and hence the emitter current and voltage are independent parameters. For the simulations reported, we use values of emitter current that were measured by Tajmar et.al[4] for a given emitter voltage. The combination of emitter current and emitter voltage used in our simulations is $10\ \mu\text{A}$ and 4.5 kV respectively.

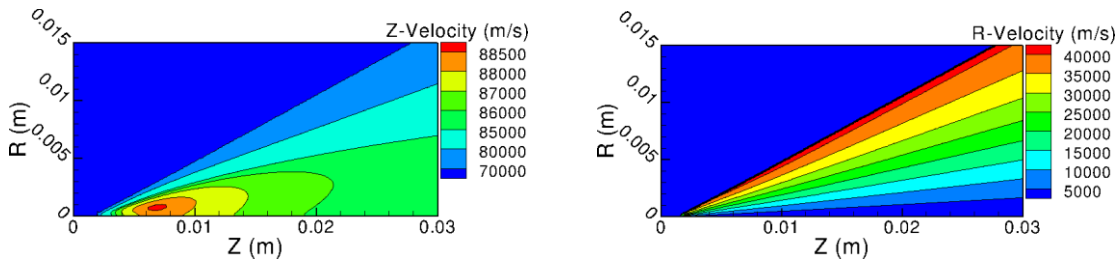


Figure 12. Contours of average ion z-velocity (left) and r-velocity (right) for the thruster operating in FEFP mode for an emitter current of 10 μ A and emitter voltage of 4.5 kV.

Figures 10 and 12 show the contours of potential and time-averaged ion velocities in z and r direction. The time-average quantities such as number density and z-velocity and r-velocity were obtained by sampling over 100,000 timesteps after reaching steady-state. In order to determine the domain size dependence on the time-averaged number density, the PIC simulations were repeated for a decreased domain size of 0.048 m \times 0.048 m and the contours obtained using the two different domain sizes are compared in Figure 13. The current density distribution obtained using the PIC simulations (shown in Figure 14(left)) were converted to current distributions that would be measured in a plane that is at a distance of 30 mm from the emitter tip. The current distributions are shown in Figure 14(right).

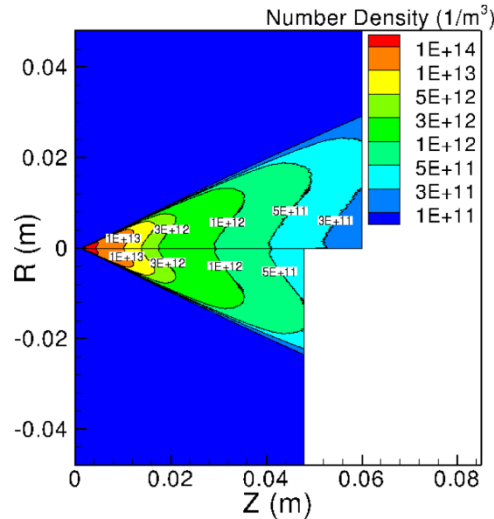


Figure 14. Contours of ion number density for two different domain sizes for the thruster operating in FEFP mode for an emitter current of 10 μ A and emitter voltage of 4.5 kV.

The results for the number density, z-velocity obtained using the PIC simulations was then used to obtain the thrust produced which is the most important performance parameter. The thrust is computed using the current density distribution as a function of radius at the plume shield plane at a distance of approximately 0.3 mm from the emitter tip. The thrust is computed using the equation

$$F = \frac{m_{ion}}{q_{ion}} \int_0^{R_{beam}} 2\pi r j(r) v_z(r) dr$$

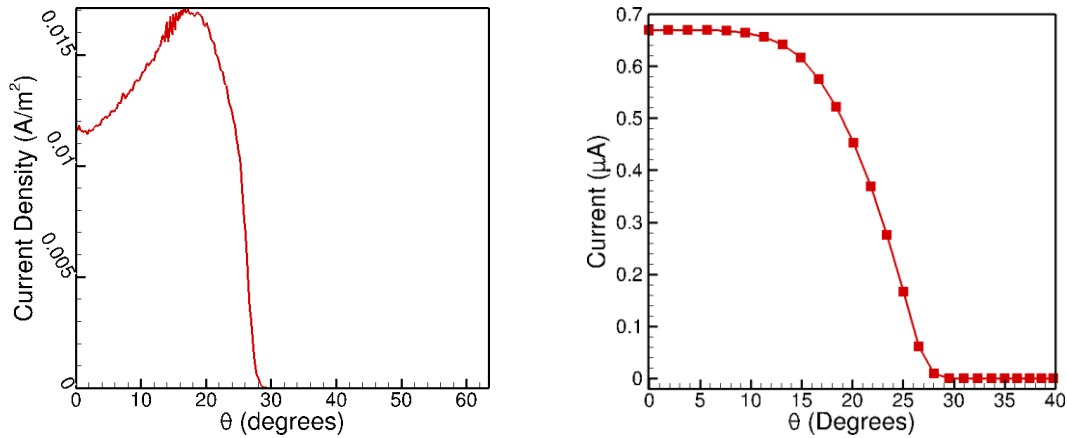


Figure 14. Angular dependence of the current density (left) and the current measured in a plane 30 mm from the emitter tip for the microthruster operating in FEFP mode for an emitter current of 10 μA and emitter voltage of 4.5 kV.

The value of R_{beam} is about 0.72 mm and the numerical integration is performed using a trapezoidal rule and the thrust is obtained as 0.94 μN which is in good agreement with the reported value of 0.80 μN . It should be mentioned that the reported value is an estimated value by the experimentalists and not a measured value.

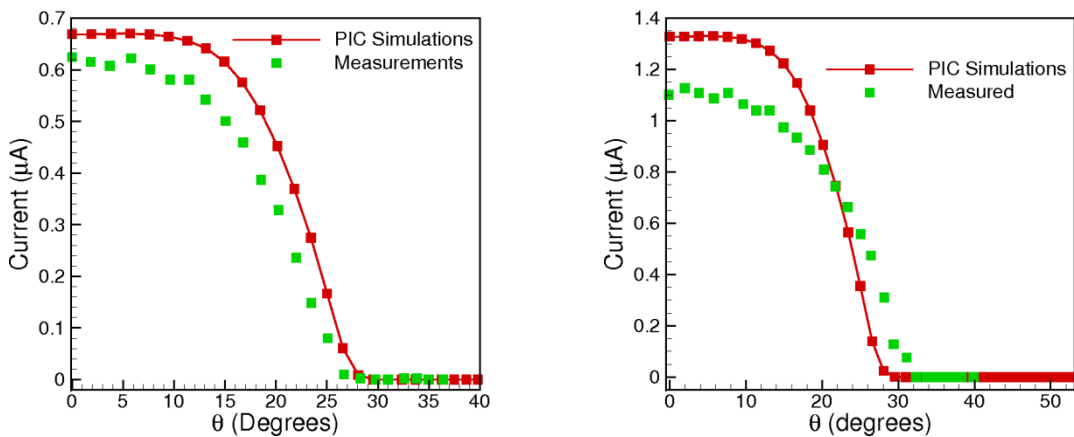


Figure 15. Angular dependence of measured [4] and simulated current in a plane 30 mm from the emitter tip for the microthruster operating in FEFP mode for a thrust of 0.8 μN (left) and 1.6 μN (right).

There are also current measurements [4] as a function of angle from the axis of symmetry for various values of emitter current and voltage and therefore various thrust levels. Figure 15 shows a comparison of the measured and simulated angular distribution of current for the two lowest thrust levels in the experiments. The agreement is good not just for normalized current but also for dimensional current. When the thrust levels are increased by increasing the emitter voltage and hence current, the neutral efflux from the emitter tip increases leading to larger beam divergence than that predicted by the PIC simulations. At the higher thrust levels, the collisions between the ions and the neutral atoms should be considered for making accurate predictions of the angular current distribution

IV. Conclusions

A micro-spike hybrid propulsion concept that consists of a combination of chemical and electric propulsion modes is proposed. The chemical mode uses a plug-annular cold/warm gas thruster with the electric mode using a field emission electric propulsion thruster housed within the plug. A computational framework that uses existing DSMC and PIC solvers is developed to analyze the performance of the dual-mode hybrid microthruster. Simulations were performed for the microthruster operating in both modes. The DSMC simulations performed for the chemical mode showed that inclusion of a centerbody in a conventional

nozzle increased Isp by at least 10 per cent for low Reynolds number flows in a non- optimized configuration with promise of increased performance with further effort. The PIC simulations performed for the FEEP mode for beam current and voltages that were taken from previous experiments predict the current density distribution, z-velocity, and hence thrust and Isp accurately. The numerical tools presented and the results obtained can be used in the design of these hybrid microthrusters by optimizing various critical performance parameters.

References

¹L.K. Yoneshige, L.E.S Ramirez, and C.F.M. Coimbra, “Microthruster Propulsion”, *Emergence of Pico- and Nanosatellites for Atmospheric Research and Technology Testing*, Progress in Aeronautics and Astronautics, vol. 234, 2010, pp.175-193.

²A.A. Alexeenko, A. Venkatraman, D. Peroullis, “Focused Solar Ablation: A Nanosat-Based Method for Active Removal of Space Debris””, Proceedings of 2010 NASA JPL/AFRL Advanced Propulsion Workshop, Nov. 15-17, 2010, Colorado Springs, CO.

³W.B.Stein, A.A. Alexeenko, I.Hrbud, D.L. Hitt, “Method of Enhancing Microthruster Performance”;United States Patent Application No. US 2010/0058734 A1 Mar. 11, 2010

⁴Tajmar, M., Genovese, A., and Steiger, W., “Indium field emission electric propulsion microthruster experimental characterization,” *Journal of Propulsion and Power*, Vol. 20, No. 2, 2004, pp. 211–218.

⁵Tajmar, M., “MEMS indium FEEP thruster: Manufacturing study and first prototype results,” *AIAA Paper*, Vol. 3619, 2004.

⁶Stein, W. and Alexeenko, A., “Application of the DSMC Method for Design of a Coaxial Microthruster Nozzle,” *AIAA Paper* 2008-4530, 2008.

⁷F. Ceccanti, L. Paita, U. Cesari, M. De Tata, N. Giusti, P. Balducci, and M. Del Pistoia Alta SpA, Pisa, 56121, Italy and D. Nicolini and L. Di Napoli, “3200 hours Endurance Testing of the Lisa Pathfinder FT-150 Thruster”; Paper IEPC-2009-170 presented at the 31st International Electric Propulsion Conference, Ann Arbor, MI, Sep. 20 – 24, 2009.

⁸J. Mueller, J. Ziemer, R. Hofer, R. Wirz, and T. O’Donnell, “A Survey of Micro-Thrust Propulsion Options for Microspacecraft and Formation Flying Missions” *Jet Propulsion Laboratory California Institute of Technology* April 9, 2008 5th Annual CubeSat Developers Workshop San Luis Obispo, CA.

⁹Bird, G. A., *Molecular Gas Dynamics and the Direct Simulation of Gas Flows*, Oxford University Press, New York, 2nd ed., 1994.

¹⁰M.S.Ivanov, A.V.Kashkovsky, S.F.Gimelshein, G.N.Markelov, A.A.Alexeenko, Ye.A.Bondar, G.A.Zhukova, S.B.Nikiforov, and P.V.Vaschenkov, “SMILE System for 2D/3D DSMC Computations,” 25th International Symposium on Rarefied Gas Dynamics, St.Petersburg, Russia, 2006.

¹¹Bradford Engineering, “Proportional Micro Thruster”: URL: http://www.bradford-space.com/pdf/be_datasheet_pmt_sep2006.pdf

¹²W. A. deGroot, “Propulsion Options for Primary Thrust and Attitude Control of Microspacecraft”, NASA/CR—1998-206608. URL: <http://gltrs.grc.nasa.gov/reports/1998/CR-1998-206608.pdf>

¹³Marotta, “Cold Gas Microthruster”: URL: https://wiki.umn.edu/pub/AEM_Air_Launch_Team/ComponentList/cold-gas-micro-thruster-article.pdf

¹⁴Birdsall, ., “Particle-in-Cell Charged-Particle Simulations, Plus Monte Carlo Collisions With Neutral Atoms, PIC-MCC,” *IEEE TRANSACTIONS ON PLASMA SCIENCE*, Vol. 19, No. 2, 1991.

¹⁵Verboncoeur, J., Langdon, A., and Gladd, N., “An object-oriented electromagnetic PIC code,” *Computer Physics Communications*, Vol. 87, No. 1-2, 1995, pp. 199–211.